X-ray Structures of the MgADP, MgATPγS, and MgAMPPNP Complexes of the *Dictyostelium discoideum* Myosin Motor Domain[†,‡]

Andrew M. Gulick, Cary B. Bauer, James B. Thoden, and Ivan Rayment*

Institute for Enzyme Research and Department of Biochemistry, University of Wisconsin, Madison, Wisconsin 53705

Received May 28, 1997; Revised Manuscript Received July 25, 1997[⊗]

ABSTRACT: The three-dimensional structures of the truncated myosin head from *Dictyostelium discoideum* myosin II (S1dC) complexed with MgAMPPNP, MgATPγS, and MgADP are reported at 2.1, 1.9, and 2.1 Å resolution, respectively. Crystals were obtained by cocrystallization and were isomorphous with respect to those of S1dC·MgADP·BeF_x [Fisher, A. J., et al. (1995) *Biochemistry 34*, 8960−8972]. In all three structures, the electron density for the entire nucleotide was clearly discernible. The overall structures of all three complexes are very similar to that of the beryllium fluoride complex which suggests that the differences in the physiological effects of ATPγS and AMPPNP are due to the changes in the equilibrium between the actin-bound and actin-free states of myosin caused by the lower affinity of AMPPNP for myosin. In S1dC·MgAMPPNP, the presence of the bridging nitrogen prompts the side chain of Asn^{233} to rotate which disrupts the hydrogen bonding pattern in the nucleotide binding pocket and alters the water structure surrounding the ribose hydroxyl groups. It appears that this change is responsible for the reduced affinity of AMPPNP for myosin relative to ATPγS. In contrast to the G-proteins, there is no major change in the conformation of the ligands that coordinate the nucleotide in S1dC·MgADP. This is due to three water molecules that adopt the approximate positions of the three oxygens on the γ-phosphate and maintain the interactions with the Mg^{2+} ion and protein molecule. Interestingly, the thiophosphate group is evident in S1dC·MgATPγS even though it is slowly hydrolyzed by myosin. This suggests that the conformation observed here and in chicken skeletal myosin subfragment-1 [Rayment, I., et al. (1993) *Science 261*, 50−58] is unable to hydrolyze ATP and represents the structure of the prehydrolysis weak binding state of myosin.

Myosin is a molecular motor that converts chemical energy into directed movement. It generates force in a unidirectional manner relative to filamentous actin through the hydrolysis of ATP. This is a cyclic process in which the binding of ATP first reduces the affinity of myosin for actin, after which hydrolysis occurs (*2*). Interestingly, the hydrolysis event occurs when myosin has little affinity for actin and leaves the molecule in a metastable state where the enzyme retains the hydrolysis products with an equilibrium constant of approximately unity between ATP and ADP·Pi in the absence of actin (*2*−*4*). The energy transduction event occurs as myosin rebinds to actin and phosphate is released (*5*). The nucleotide and actin binding activities (at least those associated with force generation) are all associated with a globular section (head) of the molecule that is common to all members of the myosin superfamily of proteins (*6, 7*) and is sufficient to generate force in an *in vitro* motility assay (*8*).

Kinetic studies suggest that the myosin head undergoes a distinct series of conformational changes during the contractile cycle depending on the state of the bound nucleotide and its interactions with actin (*9*). These conformational changes have been identified from changes in the spectroscopic and chemical properties of myosin (*4, 10*). Although the early model of Lymn and Taylor (*2*) for the contractile cycle required that myosin be either tightly bound or dissociated from actin, it subsequently became clear that a more accurate description of the system requires the introduction of additional states usually defined as strongly and weakly bound states (*11*−*13*). This was necessary because of the observation that ATP hydrolysis still occurs when myosin is associated with actin (*11*). In this revised kinetic model, weakly bound states of the actomyosin interaction are occupied by such species as myosin·ATP and myosin·ADP·P_i, whereas the strongly bound states are found when myosin binds to actin in the absence of nucleotide or in the presence of ADP (*14*). The energy transduction step then occurs during the transition from a weakly bound state to the strongly bound state. Considerable effort has been devoted to determining the relationship between the contents of the active site, the conformation of the protein and its affinity for actin (*15, 16*). This has proved to be a complex problem because of a lack of knowledge of the structural changes that accompany these transitions. For example, until recently, it was unknown if the strongly bound state of myosin for actin was the same in the presence or absence of ADP; however, at least for smooth muscle and nonmuscle myosin subfragment-1, it has now been shown that there is an additional conformational change in the myosin head on the release of ADP (*17, 18*). Likewise, many questions about the nature of the weakly bound state remain.

[†] This research was supported in part by NIH Grant AR35186 to I.R. and HFSP Grant RG33-495 to I.R., and A.M.G. was supported by NSRA Fellowship AR0842.

[‡] The X-ray coordinates have been deposited in the Brookhaven Protein Data Bank under files names 1MMG, 1MMN, and 1MMA for the MgATPγS, MgAMPPNP, and MgADP complexes, respectively.

* To whom correspondence should be addressed at the Institute for Enzyme Research, 1710 University Ave., Madison, WI 53705. Phone: (608) 262-0529. Fax: (608) 265-2904. E-mail: ivan@enzyme.wisc.edu.

[⊗] Abstract published in *Advance ACS Abstracts,* September 15, 1997.

S0006-2960(97)01259-2 CCC: $14.00

Nonhydrolyzable analogs of ATP, such as AMPPNP and ATPγS, have proved to be very useful for dissecting the biochemical properties of actomyosin by providing a way of halting the contractile cycle prior to the hydrolysis step and have allowed the early steps in the contractile cycle to be investigated (*10*, *14*, *19*−*21*). These ATP analogs have been used extensively in structural and physiological studies of muscle fibers and myofibrils (*22*−*27*). From these studies, it has been concluded that ATPγS is a good analog of the weakly bound state, whereas AMPPNP is similar in behavior to ADP and represents a strongly bound state. However, it has been unclear whether the differences in binding affinity of myosin for actin in the presence of AMPPNP or ATPγS are due to different structures of the myosin head when each of the respective nucleotide analogs is bound or whether the differences are due to the ability of the two nucleotides to affect the equilibrium between the same structural states. In the latter case, ATPγS would shift the population to weakly bound states whereas AMPPNP would leave the population in conformations that are tightly associated with actin because of the lower affinity for AMPPNP.

Given the essential role that nonhydrolyzable analogs have played in the development of the current understanding of muscle function at a physiological and biochemical level, it is important to know the detailed molecular structures of myosin when bound to these analogs. We report here the structures of the MgATPγS, MgAMPPNP, and MgADP complexes of the truncated head of *Dictyostelium discoideum* myosin II at 1.9, 2.1, and 2.1 Å resolution, respectively. This study complements the earlier structures of the truncated myosin head of *Dictyostelium* myosin complexed with MgADP·BeF_x[1,2] and MgADP·AlF_4^- and MgADP·VO_4 which mimic the ATP and transition states, respectively (*28*, *29*). This study also shows that the structure of chicken skeletal myosin subfragment-1 (*30*) represents a weakly binding conformation for the myosin head.

MATERIALS AND METHODS

Protein Purification and Crystallization. Truncated myosin subfragment-1, residues Asp^2−Asn^{762}, from *D. discoideum* (S1dC) was purified as described previously (*28*, *31*). Crystals of MgAMPPNP, MgATPγS, and MgADP complexed with S1dC were grown by microbatch from 8.3% PEG 8000, 50 mM Hepes (pH 7.0), 125 mM NaCl, 3 mM DTT, 1.2 mM $MgCl_2$, and 1.2 mM nucleotide. The protein concentration in the final droplet was about 5 mg/mL. The protein/precipitant solutions were microseeded from previous batch experiments by streak-seeding with a cat whisker (courtesy of Kappa Rayment) and left at 4 °C. Small crystals generally appeared overnight and typically took approximately 2 weeks to reach maximum dimensions of 0.6 × 0.4 × 0.15 mm.

[1] Abbreviations: myosin S1, myosin subfragment-1; S1dC, *D. discoideum* myosin motor domain; MgPPi·S1dC, magnesium pyrophosphate complex of the truncated *D. discoideum* myosin motor domain; EG, ethylene glycol; MgADP·BeF_x·S1dC, beryllium fluoride−ADP complex of the *D. discoideum* myosin motor domain; MgADP·AlF_4·S1dC, aluminum fluoride−ADP complex of the *D. discoideum* myosin motor domain; MgADP·VO_4·S1dC, vanadate−ADP complex of the *D. discoideum* myosin head; S1, subfragment-1; rms, root mean square.

[2] The exact composition of the beryllium fluoride species is unknown (*1*), but is believed to be a mixture of hydroxyfluorides; consequently, this complex will be designated BeF_x.

Table 1: Data Collection Statistics

	AMPPNP	ATPγS	ADP
X-ray source	CHESS F-1 CCD	CHESS F-1 CCD	SSRL 7-1 MAR
no. of crystals used	1	1	1
maximum resolution (d_{min}, Å)	2.1	1.9	2.1
total reflections	244 680	310 844	189 699
independent reflections	58 467	77 182	56 984
theoretical no. of reflections	63 158	79 319	59 213
completeness (%)	92.6	97.3	96.2
completeness in the highest shell[a]	55.8	91.6	90.5
R_{merge} (%)	7.5	5.7	4.6
R_{merge} (%) in the highest shell[a]	13.3	27.4	19.6
average I/σ	14.0	12.6	17.6
unit cell parameters			
a (Å)	103.9	103.8	103.6
b (Å)	180.1	179.9	179.0
c (Å)	54.1	54.0	53.9

[a] The highest-resolution shell is as follows: 2.18−2.10 Å (AMPPNP), 1.97−1.90 Å (ATPγS), and (ADP) 2.19−2.10 Å.

Crystals were almost isomorphous with respect to the earlier crystals of S1dC·MgADP·BeF_x (*28*) and belonged to the space group $P2_12_12$ (Table 1). Data were collected at −160 °C by transferring crystals incrementally from mother liquor to a cryoprotectant solution of 15% PEG 8000, 25% ethylene glycol, 300 mM NaCl, and 50 mM Hepes at pH 7.0. The crystal was then removed from the solution with a loop of surgical suture and transferred to a stream of cold nitrogen gas where it was flash-cooled (*32*, *33*).

Data Collection and Refinement. The overall strategy for data collection and refinement was similar for all three nucleotide complexes. Data were collected with synchrotron radiation from either the Cornell High Energy Synchrotron Source or the Stanford Synchrotron Radiation Laboratory, reduced, merged, and scaled with the programs DENZO and SCALEPACK (*34*). The data collection statistics for all three structures are shown in Table 1. Initial models were derived by molecular replacement with the program AMORE (*35*) from a refined S1dC structure from which the nucleotide and solvent atoms had been removed. Molecular replacement was used to position the initial models in their cells because of the differences in the cell dimensions (and presumably movements of the molecules in the lattice) induced by flash-cooling. Direct refinement, starting from a previous structure, failed to produce satisfactory convergence. The temperature factors were set to 25.0 $Å^2$ for all atoms prior to initial refinement. Least-squares refinement and manual model building were performed with the programs TNT (*36*) and FRODO (*37*), respectively. Solvent molecules were built in manually with FRODO or were identified with the program PEKPIK of the CCP4 package (*38*). After the initial stages of refinement, the locations of the nucleotides were clearly identifiable and were built into the active sites. The quality of the models was assessed with PROCHECK (*39*) and the PHIPSI program of the TNT package. The specific details of data collection for each of the three complexes are described below, whereas overall refinement statistics are given in Table 2.

MgAMPPNP. Data were collected at beamline F-1 at the Cornell High Energy Synchrotron Source (CHESS) from a single crystal in two scans with a Princeton 2K detector (*40*). The high-resolution scan consisted of 116 frames of 0.8° oscillations for 20 s and was recorded at a crystal to detector distance of 77 mm. The low-resolution scan utilized 75

Table 2: Refinement Statistics

	AMPPNP	ATPγS	ADP
total atoms	6320	6240	6139
no. of protein atoms	5811	5864	5687
no. of solvent molecules	477	337	414
av *B*-factor (Å^2)	37.4	42.3	47.3
av *B* of the protein (Å^2)	37.4	42.6	47.5
av *B* of the main chain (Å^2)	33.9	39.3	45.4
av *B* of H_2O (Å^2)	38.5	37.2	44.6
crystallographic *R*-factor (%)	19.8	22.6	21.9
weighted rms deviation			
bond lengths (Å)	0.017	0.018	0.016
bond angles (deg)	2.59	2.69	2.52
trigonal planes (Å)	0.006	0.007	0.009

frames of 1.25° for 5 s and was recorded at a crystal to detector distance of 110 mm. The mosaicity of the crystal was 0.356°. The high-resolution scan was processed to 2.0 Å, while the low-resolution data were processed to 2.7 Å. Although the completeness of the data dropped off quickly beyond 2.2 Å, the data were of sufficient quality to allow refinement against data to 2.1 Å. An initial model was obtained by molecular replacement with the program AMORE (*35*) starting from the S1dC·MgADP·BeF_x, from which water and nucleotide atoms had been removed. The model was then subjected to 30 cycles of least-squares refinement, which lowered the initial *R*-factor from 36 to 26.0%. After the next cycle of model building and refinement, the *R*-factor dropped to 24.6% and it was possible to build the Mg^{2+} ion and nucleotide into the active site. Continued refinement and model building reduced the *R*-factor to the final value of 19.8%. Analysis of the final model with PROCHECK shows that 91.5 and 8.2% of the residues lie in the fully allowed and allowed regions, respectively. Two residues, Thr^{274} and Asn^{711}, lie in the generously allowed region.

MgATPγS. Data were collected at CHESS utilizing high- and low-resolution scans with a Princeton 2K detector (*40*). The high-resolution scan included 118 frames of 0.8° for 15 s recorded at a crystal to detector distance of 77 mm, whereas the low-resolution scans consisted of 60 frames of 1.5° oscillation at 5 s per frame and were recorded at a crystal to detector distance of 117 mm. The mosaicity of the crystal was 0.275°. The high-resolution scan was processed to 1.9 Å, while the low-resolution was processed to 3.0 Å. A starting model for molecular replacement was derived from the structure of S1dC·MgADP·BeF_x, from which non-protein atoms were removed and temperature factors were reset to 25.0 Å^2. The initial *R*-factor of 41.6% dropped to 27.4% following 20 cycles of least-squares refinement. At this point, 130 waters and the nucleotide were built into the model. The geometry constraints on the γ-thiophosphate group bond lengths and angles were reduced to allow the identification of the sulfur atom. Continued model building and refinement reduced the *R*-factor to 22.6%. Analysis of the final model with PROCHECK shows that 90.8 and 8.8 of the residues lie in the fully allowed and allowed regions, respectively. Three residues, Thr^{274}, Ala^{363}, and Asn^{711}, lie in the generously allowed region.

MgADP. Data were collected at beamline 7-1 of the Stanford Synchrotron Radiation Laboratory (SSRL) with a MAR 30 cm image plate detector at a distance of 210 mm. A single scan of 76 frames was performed utilizing oscillations of 1° at a constant dosage. The mosaicity of the crystal was 0.14°. The starting model was derived from the structure of S1dC·MgAMPPNP, from which waters and nucleotide atoms were removed, and was subjected to two cycles of TNT refinement and then to five cycles of rigid body refinement during which residues Asn^2−Ile^{685} and Arg^{686}−Glu^{759} were treated as two rigid bodies. The temperature factors were then reset to 30.0 and refined through 10 cycles of least-squares refinement. After another cycle of model building and least-squares refinement, MgADP was built into the active site. Further refinement reduced the *R*-factor to the final value of 21.9%. Analysis of the final model with PROCHECK shows that 83.5 and 15.5% of the residues lie in the fully allowed and allowed regions, respectively. There are outliers, Glu^{735} and Thr^{742}, that lie in the disordered COOH-terminal region of the molecule.

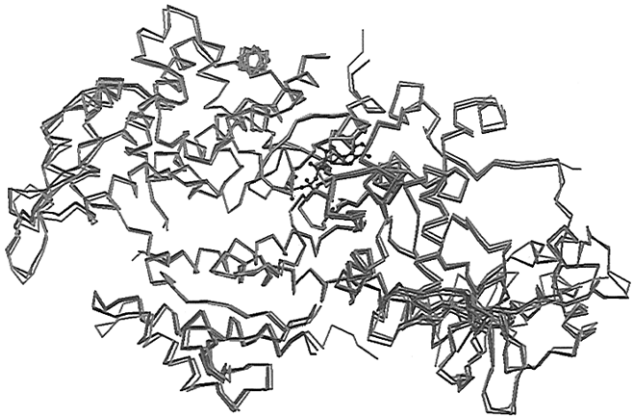

FIGURE 1: Superposition of the α-carbon tracings for the three S1dC·nucleotide complexes. The MgAMPPNP complex is shown in red, MgADP in green, and MgATPγS in blue. The protein backbones were aligned with the program LSQKAB implemented in the CCP4 program package (*38, 60*) where all Cα were included in the calculation. Figures 1−4, 6, and 7 were generated with MOLSCRIPT (*61*).

The refinement *R*-factors are somewhat higher for the MgADP and MgATPγS complexes than for the MgAMPPNP complex because of partial disorder in the small domain at the 75 NH_2-terminal and the 73 COOH-terminal residues. This appears, as discussed below, to be related to the extent of shrinkage of the *c*-axis during the rapid cooling of the crystals

RESULTS AND DISCUSSION

Comparison of the S1dC·Nucleotide Structures. The three-dimensional structures of the S1dC myosin head from *Dictyostelium* complexed with two nonhydrolyzed analogs MgAMPPNP and MgATPγS and the product of nucleotide hydrolysis, MgADP, were determined at high resolution. The final protein nucleotide models contain the following protein residues: MgAMPPNP (737 amino acids), residues Asn^2−Gly^{201}, Gly^{209}−Ile^{499}, Asp^{509}−Ala^{621}, and Phe^{627}−Glu^{759}; MgATPγS (741 amino acids), residues Asn^2−Asn^{203}, Gly^{209}−Asn^{500}, Leu^{508}−Ala^{621}, and Phe^{627}−Glu^{759}; and MgADP (719 amino acids), residues Asn^2−Asp^{23}, Asp^{31}−Gln^{204}, Gly^{209}−Glu^{497}, Ile^{504}−Ala^{621}, Asn^{626}−Phe^{701}, and Gln^{720}−Glu^{759}. The final refinement statistics are given in Table 2.

The overall protein conformation is very similar for all three nucleotide complexes as seen from the overlap of their α-carbons in Figure 1. As noted previously in the comparison of the BeF_x and AlF_4 complexes of S1dC (*28*), there is more conformational flexibility in the NH_2 and COOH

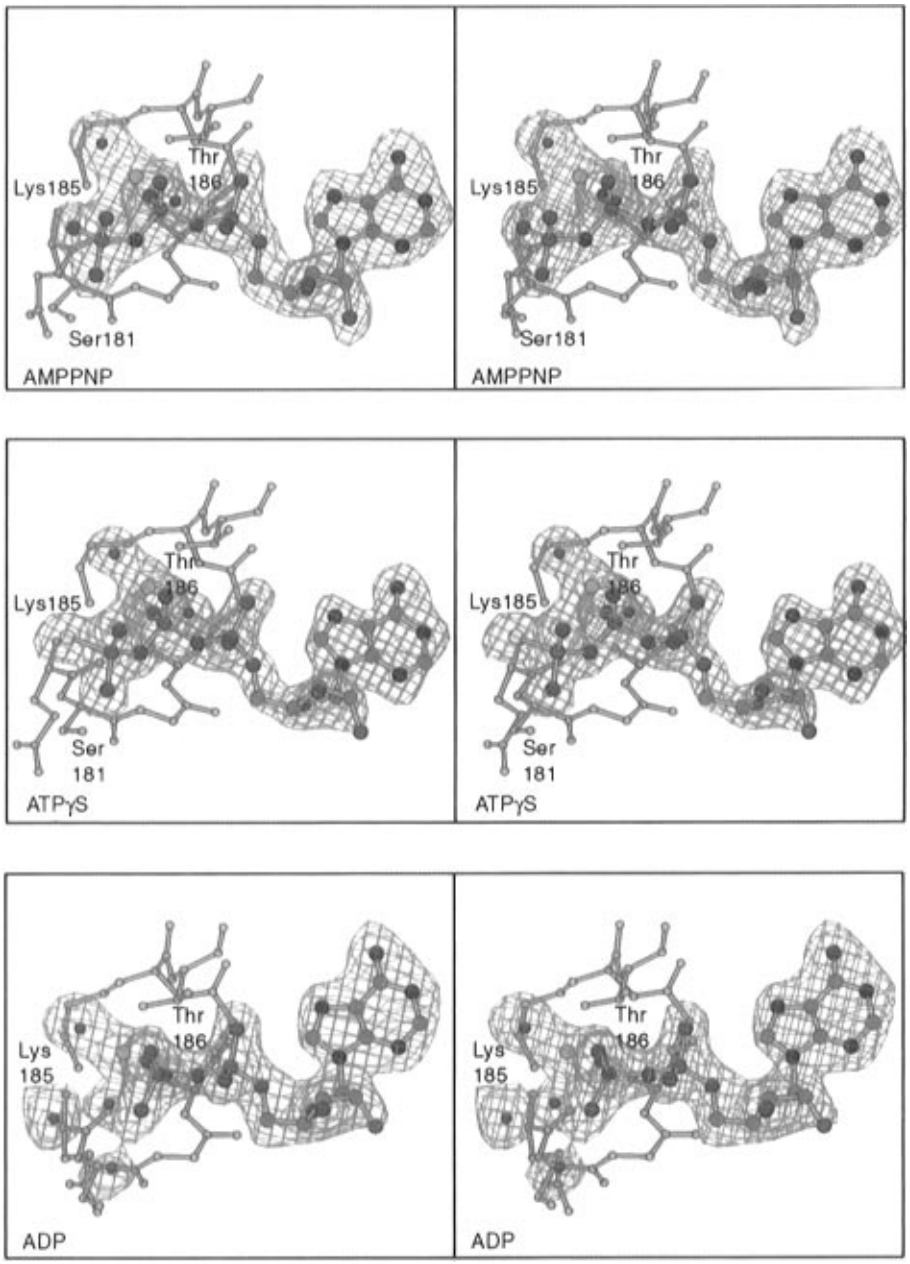

FIGURE 2: Stereoview of the electron density associated with the nucleotide binding site. The P-loop residues Glu^{180}–Thr^{186} are included in each figure. The electron density was calculated from $F_o - F_c$ coefficients where the nucleotides were excluded from refinement and phase calculation: (a) MgAMPPNP, (b) MgATPγS, and (c) MgADP. The electron density was included in the figure using the programs FRODO (*37*) and MOLDED (A. J. Fisher, unpublished results).

Table 3: rms Differences in Angstroms[a]

	ADP·BeF_x	AMPPNP	ATPγS
AMPPNP	0.45		
ATPγS	0.38	0.25	
ADP	1.17	1.10	1.09

[a] The rms difference was calculated with the program LSQKAB implemented in the CCP4 program package (*38*, *60*) for the α-carbon atoms of the two protein structures being compared.

domains of the proteins than in the central section of the polypeptide chain. This phenomenon is also observed in the complexes reported here where the majority of the differences in the tertiary structures are located in NH_2 and COOH domains. The rms difference for the three structures is reported in Table 3, as well as a comparison to the earlier structure of S1dC·MgADP·BeF_x (*28*). There are small local differences between the three ATP-like complexes, ADP·BeF_x, AMPPNP, and ATPγS. The largest difference in rms value arises in the comparisons between the ATP-like complexes and the S1dC complex with MgADP. As can be seen in Figure 1, however, this difference results from an overall minor change in the protein structure rather than from a large movement of a single domain. Indeed, the rms differences between the MgADP and MgAMPPNP complexes in the upper and lower domains of the 50 kDa region are 1.08 and 0.76 Å, respectively, whereas the rms difference for the NH_2-terminal domains is only 0.26 Å. This difference appears to arise as a consequence of the variability in the cell dimensions induced by flash-cooling the crystals. It has been observed that when the *c*-axis shrinks below 180 Å disorder is induced into the NH_2- and COOH-terminal regions of the protein. This poses problems in refining such structures, since it is difficult to model this disorder and as a consequence it typically prevents the crystallographic

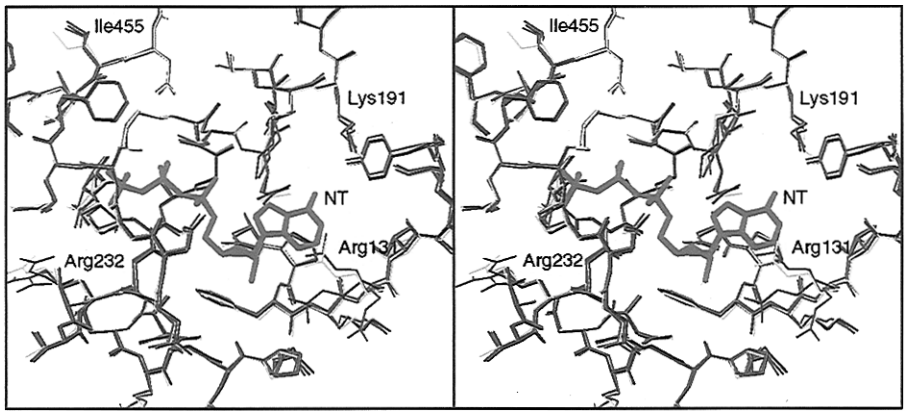

FIGURE 3: Stereoview of an overlay of nucleotide binding pockets. The active sites for the S1dC complexes with MgAMPPNP (red), MgADP (green), MgATPγS (blue), and MgADP·BeF_x (yellow) are shown. A molecule of AMPPNP is shown in cyan. The alignment was made with the program LSQKAB implemented in the CCP4 program package (*38*, *60*) by fitting the residues surrounding the nucleotide pocket: Asn^{127} − Tyr^{135}, Glu^{180} − Asn^{188}, Thr^{230} − Arg^{238}, and Asp^{454} − Gly^{457}. The side chains that exhibit the most movement are labeled.

R-factor from decreasing below 21%. In the MgADP structure, the dimension of the *c*-axis (179.0 Å) is quite low; it is likely the source of the greater rms difference. Nonetheless, the electron density in the vicinity of the nucleotide is unequivocal and fully supports the conclusions drawn here.

Nucleotide Binding Pockets in the Different Nucleotide Complexes. The electron density of the different nucleotide complexes clearly indicates the orientation of the substrate molecule in the active site (Figure 2). The nucleotides bind in the same orientation as that observed previously for the MgADP·BeF_x complex. The nucleotide base lies in a cavity bordered by residues Phe^{129}−Tyr^{135} and Glu^{187}−Lys^{191}. Few direct interactions are formed, most notably a hydrogen bond formed between the side chain of Tyr^{135} and between the C6-amino group of the adenine ring. There are also indirect hydrogen bonds made through intervening water molecules between N1 of the adenine ring and both the carbonyl and amide nitrogen of Ile^{132} and between N7 of the adenine ring and the side chain of Asn^{188}. There are few interactions made to the ribose moiety of the nucleotide. The 2′- and 3′-hydroxyls point away from the protein molecule, an orientation which allows them to be modified by a variety of chemical groups and yet still bind in the active site (*41*). A hydrogen bond is formed between the side chain of Asn^{127} and the ribose ring oxygen.

The phosphate binding region of the three complexes is the most interesting aspect of the new structures. The three nucleotides differ by the presence of the β,γ-imido substitution in AMPPNP, the γ-thio substitution in ATPγS, and the lack of a γ-phosphate group altogether in ADP. There are, in fact, very few changes in the protein atoms that make up the nucleotide binding pocket (Figure 3). The rms differences in all atoms in the residues that line the nucleotide pocket (residues Asn^{127}−Tyr^{135}, Glu^{180}−Asn^{188}, Asn^{233}−Arg^{238}, and Asp^{454}−Gly^{457}) are 0.65 Å between AMPPNP and ATPγS structures, 0.74 Å between AMPPNP and ADP structures, and 0.85 Å between ATPγS and ADP structures. The large differences are a result of the movement of four side chains at the active site, Arg^{131}, Glu^{180}, Arg^{232}, and Ile^{455}. Lys^{190} and Lys^{191} also show slight changes in their orientation. The side chains of Glu^{180} and Arg^{232} point away from the active site and into the solvent. Hence, it is not surprising that these side chains exhibit flexibility between the different structures. The side chain of Ile^{455} is in a hydrophobic pocket, and the three new structures all exhibit rotation about the χ_1 dihedral angle relative to the original S1dC·MgADP·BeF_x structure. Although this residue undergoes a conformational change between the prehydrolysis and transition states (*28*, *29*), it seems unlikely that the observed change would affect this function of this residue. Finally, Arg^{131} forms an ionic interaction with Glu^{187} to form a cover on the nucleotide pocket (*28*). In the three new structures, the density for this residue is weak, indicating some degree of conformational freedom. In the AMPPNP and ADP structures, it has been built in a conformation that clearly precludes this interaction with Glu^{187} (Figure 3). Exclusion of the side chains of residues Arg^{131}, Glu^{180}, Arg^{232}, and Ile^{455} from the rms calculation results in differences of 0.17 Å between the AMPPNP and ATPγS structures, 0.24 Å between the AMPPNP and ADP structures, and 0.21 Å between ATPγS and ADP. This illustrates the conserved structure of the three protein−nucleotide complexes.

A Mg^{2+} ion is present in the active site of all three complexes, as was observed for the previous S1dC·nucleotide structures (*28*, *29*). The metal ion is coordinated by six oxygen atoms. These atoms arise from two protein side chains, namely Thr^{186} and Ser^{236}, from oxygens on the β- and γ-phosphates, and from two water molecules. As described below, a third water molecule replaces the γ-phosphate oxygen in the MgADP structure. All of the interactions between the protein and nucleotide are very similar. The lengths of the various hydrogen bonds formed between the protein atoms and the phosphate oxygens are given in Table 4; the different nucleotide complexes are described below.

MgAMPPNP. There are no major changes in the structure of S1dC or the coordination of the nucleotide caused by the presence of the imido linkage in the AMPPNP substrate analog. The hydrogen bond distances to the atom bridging the β- and γ-phosphates are very similar for a bridging nitrogen in AMPPNP or for a bridging oxygen in ATPγS. However, examination of the hydrogen bonding pattern surrounding the bridging nitrogen suggests that the amido side chain of Asn^{233} has rotated relative to the arrangement seen in all other nucleotide complexes of S1dC. Consequently, Asn^{233} Oδ1 accepts a hydrogen bond from the hydrogen on the bridging nitrogen. Rotation of the amido group allows the bridging nitrogen to form two reasonable

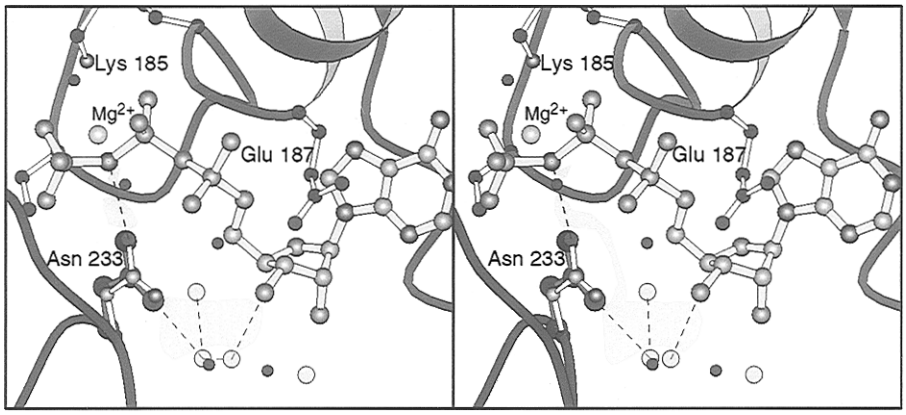

FIGURE 4: Stereoview of the hydrogen bond interaction surrounding Asn^{233} of the AMPPNP active site. Shown in yellow is MgAMPPNP, and shown in green are the P-loop residues Glu^{180} − Lys^{191} and residues Val^{126} − Arg^{131} of the AMPPNP complex. The lower left corner of the figure contains the switch I-loop which contains Asn^{233}, a residue that interacts with the $\beta-\gamma$ bridging oxygen. In the AMPPNP structure, the amido side chain is flipped to allow the side chain oxygen to interact with the bridging nitrogen. This changes the water structure from that seen in the ADP·BeF$_x$ complex (large pink water molecules) to the new structure seen with AMPPNP (small red water molecules).

Table 4: Hydrogen Bond Distances (Å) at the Phosphate Pocket[a]

atom 1	atom 2	AMPPNP	ATPγS	ADP
OB2	Mg^{2+}	2.0	2.0	2.0
OG3	Mg^{2+}	2.1	2.1	2.2 [995 Ow1]
OB1	185 Nζ	2.6	2.6	2.8
OB1	184 N	2.9	2.8	2.8
NB3	182 N	2.7	2.7 [OB3]	2.7 [OB3]
NB3	233 Oδ2	2.8	3.1 [OB3]	3.0 [OB3]
OG2	181 Oγ	2.6	2.1	2.2 [995 Ow5]
OG2	236 Oγ	2.5	2.9	2.6 [995 Ow5]
OG1	185 NZ	2.9	2.8 [SG1]	2.6 [995 Ow2]
OG3	237 N	2.7	2.8	3.2 [995 Ow1]

[a] Nucleotide atoms are listed in the first column. Where necessary, the new designation of nucleotide atoms is indicated in brackets. The second column contains protein atoms, which are designated by residue number followed by the atom name.

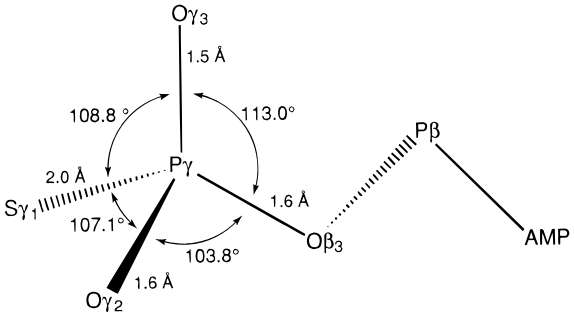

FIGURE 5: Bond lengths and angles associated with the γ-phosphate of ATPγS. The naming of the atoms is as listed in Table 4. Oγ3 is the oxygen that interacts with the Mg^{2+} ion, and Sγ1 interacts with Lys^{185} and Oγ2 with the side chain of Ser^{181}.

hydrogen bonds but now places the amino group of Asn^{233} in the location occupied previously by Oδ1 (Figure 4). This disrupts the hydrogen bond to the backbone amide hydrogen of Asn^{235} and thus alters the water structure surrounding the nucleotide, in particular surrounding the ribose hydroxyl groups. It seems likely that the rotation of the side chain of Asn^{233} is responsible for the reduced affinity of AMPPNP for myosin relative to ATPγS.

MgATPγS. Prior to the determination of the structure of the MgATPγS complex with S1dC, it was unclear if the thiophosphate group would be visible in the electron density since this analog is hydrolyzed slowly by myosin (*21*, *42*). Likewise, if present, it was unknown if it would be possible to identify a unique location for the sulfur or whether the sulfur atom would be equally distributed between the three terminal oxygen positions in the nucleotide molecule. After refinement of the initial molecular replacement solution, it was evident not only that there was density for the thiophosphate but also that there was a larger lobe of density at one of the terminal positions. The sulfur was built into this location, and in subsequent least-squares refinement, the geometric constraints were loosened for all bond lengths and angles at the γ-phosphate. The final bond lengths and angles at the γ-phosphate are shown in Figure 5. The bond length formed from the γ-phosphorus to the sulfur atom, 2.0 Å, is significantly longer than the two bonds to the oxygen atoms and is consistent with a P−S single bond. The average bond length for a phosphorus sulfur double bond in two phosphorothioate triester compounds is 1.90 Å (*43*, *44*). In diesters, where resonance distributes the negative charge between the sulfur atom and one oxygen, there is less double bond character to the phosphorus sulfur bond, and the bond length increases to 1.94 Å (*45*). Conversely, a P−S single bond distance has been observed to be 2.04 Å (*46*). Differences in the bond lengths to the remaining oxygens at the γ-phosphate are below the limits of resolution for this structure.

The sulfur atom is located within hydrogen bonding distance of the Lys^{185} ϵ-amino group (Figure 6) and is consistent with the ligands that form the major components of the γ-phosphate binding site. As seen in the MgAMPPNP complex, the three oxygens of the γ-phosphate moiety are coordinated predominately by three groups of ligands: the magnesium ion, Lys^{185}, and Ser^{236} and Ser^{181}. Given that magnesium would rather coordinate an oxygen ligand, the sulfur atom would be expected to be coordinated by one of the last two groups. Also, since the sulfur atom is more acidic than the oxygen atoms, the resonance structure with the negative charge located on the sulfur is expected to be favored. In turn, this would be expected to interact with the positive charge on the side chain of Lys^{185}. It is likely, however, that the Oγ3 oxygen which interacts with the Mg^{2+} also carries a negative charge with the favored resonance structure placing the double bond to the oxygen closest to the side chains of Ser^{181} and Ser^{236}.

MgADP. The similar conformation of the protein backbone between the prehydrolysis nucleotide analog complexes

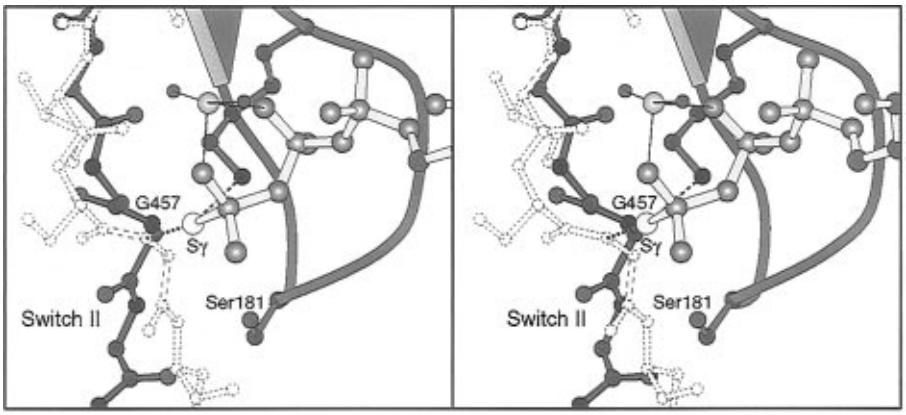

FIGURE 6: Stereoview of the γ-phosphate pocket of the S1dC·MgATPγS structure. Shown in green are the P-loop residues Ile^{177} − Lys^{185}. The switch II regions of the ATPγS (red bonds) and ADP·VO_4 (white bonds and atoms) complexes are also shown. In S1dC·MgATPγS, the Sγ interacts with the side chain of Lys^{185}. In order to attain the structure observed in S1dC·MgADP·VO_4, an additional hydrogen bond between the amide hydrogen of Gly^{457} would be required (shown in red), which is unlikely to occur.

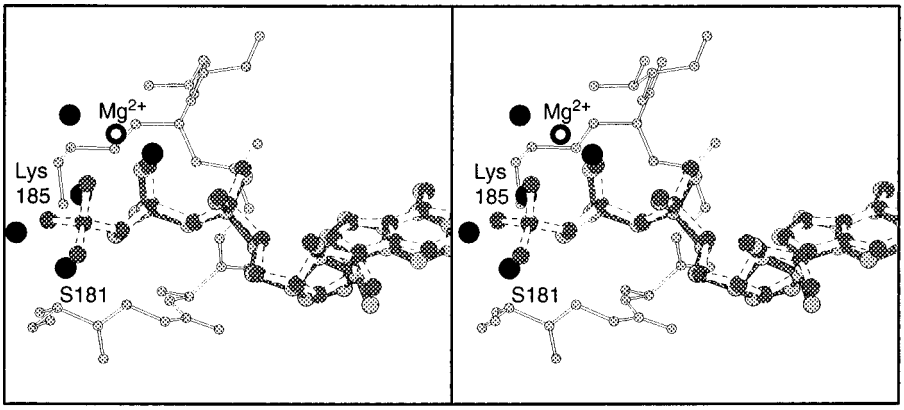

FIGURE 7: Stereoview of an overlay of the ADP and ADP·BeF_x nucleotides. Included in the figure are ADP (solid lines, light gray atoms) and ADP·BeF_x (dashed lines, dark gray atoms) and the three water molecules (black circles) from the ADP structure that approximate the location of the three γ-phosphate oxygens. The protein atoms that form the P-loop are also shown (residues Ser^{181} − Thr^{186}).

and the complex seen with MgADP (Figure 2), the product of nucleotide hydrolysis, was at first surprising. It was anticipated from the similarity between myosin and the G-proteins in the phosphate binding region (*47*) that there would be a significant change associated with the ligands surrounding the magnesium binding site since in the G-proteins a significant change occurs in the switch I region on release of the γ-phosphate (*48*). Conversely, the isomorphous nature of the protein crystals suggested that there might be little difference in the structure. The reason for the lack of conformational change appears to lie in the water structure surrounding the β-phosphate. In the active site, electron density for three water molecules was clearly visible (Figure 2C). These three water molecules are located at positions that approximate the three oxygens on the γ-phosphate (Figure 7). These water molecules maintain the interactions with the Mg^{2+} ion and protein molecule that are formed by the γ-phosphate oxygens in the prehydrolysis nucleotide complexes. As a consequence of these interactions, there are no significant domain movements observed in the S1dC protein molecule complexed with MgADP. This structure suggests that in solution the myosin·MgADP complex would be similar to that of myosin·MgATP; however, it should be noted that this complex is not expected to be a major component of the contractile cycle since the myosin·ADP complex of interest occurs when myosin is bound to actin. Under these conditions, the actomyosin·MgADP complex is clearly different from the myosin·MgATP complex since one conformation resides close to the end of the contractile cycle whereas the other represents the first stage of the cycle. The structure of S1dC·MgADP points to an important difference between the G-proteins and myosin in the way the conformations induced by hydrolysis are used for biological function. To a first approximation, the G-proteins function as switches that exist in one of two states (either the GTP or GDP state) (*48*−*50*). In contrast, myosin requires a minimum of three conformations (actomyosin, myosin·MgATP, and myosin·MgADP·P_i) in order to create a cycle from which work can be extracted. The additional state (relative to the G-proteins) represented by myosin·MgADP·P_i prepares the molecule for the power stroke that is induced when myosin rebinds to actin and releases inorganic phosphate. Thus, the myosin·MgADP complex (in solution) does not provide a critical biological function as does the MgGDP complex for the G-proteins.

The actomyosin contractile cycle is intimately associated with the timing of successive protein−nucleotide and protein−protein interactions. It is believed that conformational changes associated with the binding of ATP and subsequent hydrolysis are communicated to the actin binding interface of the myosin molecule via domain movements in the central section of the myosin head (*51*) and to the regulatory domain of the myosin head (*28*, *29*, *52*). To improve our understanding of the contractile cycle, we have investigated the structure of the truncated head from *Dictyostelium* myosin II in the presence of a series of nucleotide

molecules. The current study examines the structure of two nonhydrolyzed nucleotide analogs, AMPPNP and ATPγS, and the structure of the complex with one of the products of nucleotide hydrolysis. This study confirms that the earlier structure of S1dC·MgADP·BeF_x is indeed a good model of the prehydrolysis state; however, the most striking feature of these structures is their similarity. The similarity of the structures has implications for understanding the physiological effect of these analogs and imposes limits on the structural states available to myosin in solution.

The current description of the contractile cycle involves the transition from strongly bound states when myosin binds to actin in the absence of nucleotide to weakly bound states when ATP or the hydrolysis products are bound and back to strongly bound states as myosin rebinds to actin and products are released (*9*). There has been considerable discussion about the nature of these weakly and strongly bound states. Indeed, every available kinetic and spectroscopic tool has been applied to this problem in an attempt to understand the structure of myosin as it interacts with actin and nucleotides. All of these investigations have benefited from the use of ATPγS and AMPPNP.

Fiber studies have shown that the addition of AMPPNP to actomyosin leaves myosin in a strongly bound state, although there are changes in the tensile properties of the myofibril (*24*). This is also reflected in structural changes in insect muscle whereby AMPPNP causes the release of a subset of the myosin heads in the rigor state (*27*). In contrast, ATPγS dissociates myosin heads from actin and creates a weakly bound state (*21, 22*). Saturation-transfer electron paramagnetic spectroscopy has shown that the addition of AMPPNP to vertebrate acto-S1 does not increase the rotational mobility of the myosin head relative to that observed in the rigor state (*53*). In contrast, addition of ATPγS greatly decreases the rotational correlation time and increases the rotational flexibility of the bound S1 heads, demonstrating that in the weakly bound state myosin adopts a wide range of orientations relative to actin. Similar results were observed from proteolytic sensitivity and fluorescence assays comparing the cross-linked acto-S1 upon nucleotide addition (*20*). These studies show that ATPγS mimics the weakly bound state. Since the three-dimensional structures of S1dC when complexed to ATPγS or AMPPNP do not show any major differences, this suggests that the differences in the physiological effects of these ATP analogs are due to the changes in the equilibrium between the actin-bound and actin-free states of myosin caused by the lower affinity of AMPPNP for myosin.

The structure of S1dC·MgATPγS strongly suggests that the conformation observed in this class of complexes and also in chicken skeletal myosin subfragment-1 (*30*) is that of the prehydrolysis state and implies that this state is unable to hydrolyze ATP. The present study provides structural evidence for an initial transition from the actin-bound state to a conformation that binds weakly to actin and yet does not hydrolyze nucleotide as has been suggested from kinetics studies (*2, 9*). This point arises because the thiophosphate group is observed in the crystal lattice even though ATPγS is slowly hydrolyzed by myosin.

It is well-established that hydrolysis of ATP occurs by attack of a water molecule on the γ-phosphorus (*54*−*56*). Prior to the structural studies on myosin, it was expected that this process would involve a general base provided by an amino acid side chain that would serve to activate the water molecule by abstraction of a proton. It now appears that the ultimate base is the γ-phosphate itself since there is no group that might function as a general base within 5 Å of the terminal phosphate (*28*). It is also possible that the proton might be transferred to the terminal phosphate indirectly via hydrogen exchange through an intervening water molecule or a hydroxyl of Ser^{236} (*28*). It has been argued previously that a conformational change is required to orient the nucleophilic water molecule and configure the active site for facile hydrolysis of ATP and that this conformational change is intimately coupled to preparing the molecule for the power stroke (*28, 29*). This mechanism is analogous to the earlier observation of GTP hydrolysis with the G-proteins (*57, 58*), where a linear free energy relationship exists between the pK_a of the nucleotide and the log of the rate of the reaction (*59*). For p21ras, it was shown that the pK_a of GTPγS was nearly 0.5 pK_a unit lower than that for GTP, explaining the slow rate of hydrolysis in the unactivated reaction (*59*).

ATPγS is hydrolyzed by myosin at a steady state rate that is comparable to the intrinsic non-actin-activated steady state rate of hydrolysis for ATP (*21*, *42*) which is considerably slower than the actin activate rate for ATP hydrolysis. Interestingly, the rate of hydrolysis of ATPγS is not activated by actin (*21, 42*) which suggests that the metastable state is not attained for ATPγS and that the rate-limiting step for hydrolysis of this nucleotide is bond cleavage rather than product release as for ATP. Since the hydrolysis of MgATPγS is catalyzed by myosin (albeit at a slow rate), an obvious question is why is the electron density for the γ-phosphate evident in the crystals?

The level of the electron density for the thiophosphate group is comparable to that of the other atoms in the active site such that the occupancies were not refined; however, the temperature factors for the γ-phosphate atoms are somewhat higher than for the atoms of the α- and β-phosphates which may indicate that some of the S1dC molecules contain MgADP at the active site rather than MgATPγS. Even so, it is clear that the major species present in the crystals is ATPγS (Figure 2B). While it is conceivable that the crystals have bound to ATPγS that was present in the cryoprotectant soaking solution, similar attempts to soak ATP or any other nucleotide into crystals that were grown with PP_i have been unsuccessful. Indeed, ATP has no effect on crystals of S1dC·$MgPP_i$. In contrast, MgATP can be diffused into crystals of apo-S1dC without immediate damage (C. B. Bauer and I. Rayment, unpublished results) which suggests that the active site is accessible in the crystal lattice. This information implies that the nucleotide observed in the electron density is that present at the time of crystallization. Given the time frame of crystallization (weeks) and the significant rate of hydrolysis in solution, it would be anticipated that the thiophosphate group should be lost. This implies that the conformation of the protein in the lattice is unable to catalyze hydrolysis. In turn, this suggests that the conformation observed in the structure of S1dC·MgADP·VO_4 is necessary for catalysis of ATP hydrolysis.

As noted above, the slow rate of hydrolysis of GTPγS by ras has been attributed to its reduced pK_a relative to GTP (*59*). By analogy, this might explain the slow rate of hydrolysis of ATPγS by myosin in solution; however, in this case, structural factors may also play a role. Examina-

tion of the coordination of the thiophosphate group in the active site reveals that the sulfur atom is coordinated to Lys^{185}. In the structure of S1dC·MgADP·VO_4, which mimics the conformation at the transition state for hydrolysis, the equivalent oxygen atom forms an additional hydrogen bond to the amide nitrogen of Gly^{457} (Figure 6). The formation of this hydrogen bond appears to be a central component of the conformation that has been suggested to be necessary for catalysis and establishment of the metastable state (*28*, *29*). It is unlikely that the sulfur atom would form a strong hydrogen bond to the amide nitrogen of Gly^{457} which suggests that the conformation required for hydrolysis and formation of the metastable state would be less favorable. This might also contribute to the reduced hydrolysis rate and lack of actin activation observed for ATPγS (*42*).

CONCLUSIONS

A knowledge of the structure of myosin in its strongly bound and weakly bound states is necessary for establishing the structural foundation for myosin-based motility. The present study provides evidence that the initial weak binding state as modeled by the ATPγS complex is unable to hydrolyze ATP and that a subsequent structural transition, to the conformation observed in S1dC·MgADP·VO_4, is needed to activate the ATPase activity and prime the molecule for the start of the power stroke. This then provides a structural understanding of a contractile cycle in which the release of myosin from actin by ATP does not reverse the power stroke.

ACKNOWLEDGMENT

We thank H. M. Holden for helpful discussions and R. Smith for help with preparing the protein used in this study. We also thank A. J. Fisher and C. A. Smith who initiated attempts to collect the data reported here. We also thank the reviewers for their helpful comments.

REFERENCES

1. Henry, G. D., Maruta, S., Ikebe, M., and Sykes, B. D. (1993) *Biochemistry 32*, 10451−10456.
2. Lymn, R. W., and Taylor, E. W. (1971) *Biochemistry 10*, 4617−4624.
3. Bagshaw, C. R., and Trentham, D. R. (1973) *Biochem. J. 133*, 323−328.
4. Bagshaw, C. R., and Trentham, D. R. (1974) *Biochem. J. 141*, 331−349.
5. Goldman, Y. E. (1987) *Ann. Rev. Physiol. 49*, 637−654.
6. Cope, M. J. T. V., Whisstock, J., Rayment, I., and Kendrick-Jones, J. (1996) *Structure 4*, 969−987.
7. Sellers, J. R., Goodson, H. V., and Wang, F. (1996) *J. Muscle Res. Cell Motil. 17*, 7−22.
8. Toyoshima, Y. Y., Kron, S. J., McNally, E. M., Niebling, K. R., Toyoshima, C., and Spudich, J. A. (1987) *Nature 328*, 536−539.
9. Geeves, M. A. (1991) *Biochem. J. 274*, 1−14.
10. Trybus, K. M., and Taylor, E. W. (1982) *Biochemistry 21*, 1284−1294.
11. Stein, L. A., Schwarz, R. P. J., Chock, P. B., and Eisenberg, E. (1979) *Biochemistry 18*, 3895−3909.
12. Eisenberg, E., and Greene, L. E. (1980) *Annu. Rev. Physiol. 42*, 293−309.
13. Geeves, M. A., Goody, R. S., and Gutfreund, H. (1984) *J. Muscle Res. Cell Motil. 5*, 351−361.
14. Greene, L. E., and Eisenberg, E. (1980) *J. Biol. Chem. 255*, 543−548.
15. Goody, R. S., and Holmes, K. C. (1983) *Biochim. Biophys. Acta 726*, 13−39.
16. Cooke, R. (1986) *CRC Crit. Rev. Biochem. 21*, 53−118.
17. Hoenger, A., Sablin, E. P., Vale, R. D., Fletterick, R. J., and Milligan, R. A. (1995) *Nature 376*, 271−274.
18. Jontes, J. D., Wilson-Kubalek, E. M., and Milligan, R. A. (1995) *Nature 378*, 751−753.
19. Yount, R. G., Ojala, D., and Babcock, D. (1971) *Biochemistry 10*, 2490−2495.
20. Duong, A. M., and Reisler, E. (1989) *Biochemistry 28*, 3502−3509.
21. Resetar, A. M., and Chalovich, J. M. (1995) *Biochemistry 34*, 16039−16045.
22. Dantzig, J. A., Walker, J. W., Trentham, D. R., and Goldman, Y. E. (1988) *Proc. Natl. Acad. Sci. U.S.A. 85*, 6716−6720.
23. Fajer, P. G., Fajer, E. A., Brunsvold, N. J., and Thomas, D. D. (1988) *Biophys. J. 53*, 513−524.
24. Schoenberg, M. (1989) *Biophys. J. 56*, 33−41.
25. Berger, C. L., and Thomas, D. D. (1994) *Biophys. J. 67*, 250−261.
26. Roopnarine, O., and Thomas, D. D. (1996) *Biophys. J. 70*, 2795−2806.
27. Winkler, H., Reedy, M. C., Reedy, M. K., Tregear, R., and Taylor, K. A. (1996) *J. Mol. Biol. 264*, 302−322.
28. Fisher, A. J., Smith, C. A., Thoden, J., Smith, R., Sutoh, K., Holden, H. M., and Rayment, I. (1995) *Biochemistry 34*, 8960−8972.
29. Smith, C. A., and Rayment, I. (1996) *Biochemistry 35*, 5404−5417.
30. Rayment, I., Rypniewski, W. R., Schmidt-Bäse, K., Smith, R., Tomchick, D. R., Benning, M. M., Winkelmann, D. A., Wesenberg, G., and Holden, H. M. (1993) *Science 261*, 50−58.
31. Itakura, S., Yamakawa, H., Toyoshima, Y. Y., Ishijima, A., Kojima, T., Harada, Y., Yanagida, T., Wakabayashi, T., and Sutoh, K. (1993) *Biochem. Biophys. Res. Commun. 196*, 1504−1510.
32. Teng, T. Y. (1990) *J. Appl. Crystallogr. 23*, 387−391.
33. Rodgers, D. W. (1994) *Structure 2*, 1135−1140.
34. Otwinowski, Z. (1986) Ph.D. Thesis, Yale University, New Haven, CT.
35. Navaza, J. (1993) *Acta Crystallogr. D 49*, 588−591.
36. Tronrud, D. E., Ten Eyck, L. F., and Matthews, B. W. (1987) *Acta Crystallogr. A 43*, 489−501.
37. Jones, T. A. (1985) in *Methods in Enzymology* (Wycoff, H. W., Hirs, C. H. W., and Timasheff, S. N., Eds.) Vol. 115, pp 157−171, Academic Press Inc., New York.
38. CCP4 (1994) *Acta Crystallogr. D 50*, 760−763.
39. Laskowski, R. A., MacArthur, M. W., Moss, D. S., and Thornton, J. M. (1993) *J. Appl. Crystallogr. 26*, 283−291.
40. Walter, R. L., Thiel, D. J., Barna, S. L., Tate, M. W., Wall, M. E., Eikenberry, E. F., Gruner, S. M., and Ealick, S. E. (1995) *Structure 3*, 835−844.
41. Yount, R. G., Cremo, C. R., Grammer, J. C., and Kerwin, B. A. (1992) *Philos. Trans. R. Soc. London, Ser. B 336*, 55−61.
42. Goody, R. S., and Mannherz, H. G. (1975) in *Protein-Ligand Interactions* (Sund, H., and Blauer, G., Eds.) de Gruyter, Berlin.
43. Baughman, R. G., and Jacobson, R. A. (1976) *J. Agric. Food Chem. 24*, 1036−1041.
44. Baughman, R. G., and Yu, P.-J. (1982) *J. Agric. Food Chem. 30*, 293−295.
45. Burgers, P. M. J., Sathyanarayana, B. K., Saenger, W., and Eckstein (1979) *Eur. J. Biochem. 100*, 585−591.
46. Roschenthaler, G.-V., Bohlen, R., and Schomburg, D. (1985) *Z. Naturforsch., B: Chem. Sci. 40*, 1589.
47. Smith, C. A., and Rayment, I. (1996) *Biophys. J. 70*, 1590−1602.
48. Milburn, M. V., Tong, L., DeVos, A. M., Brünger, A., Yamaizumi, Z., Nishimura, S., and Kim, S.-H. (1990) *Science 247*, 939−945.
49. Coleman, D. E., Berghuis, A. M., Lee, E., Linder, M. E., Gilman, A. G., and Sprang, S. R. (1994) *Science 265*, 1405−1412.
50. Mixon, M. B., Lee, E., Coleman, D. E., Berghuis, A. M., Gilman, A. G., and Sprang, S. R. (1995) *Science 270*, 954−960.

51. Rayment, I., Holden, H. M., Whittaker, M., Yohn, C. B., Lorenz, M., Holmes, K. C., and Milligan, R. A. (1993) *Science 261*, 58−65.
52. Fisher, A. J., Smith, C. A., Thoden, J., Smith, R., Sutoh, K., Holden, H. M., and Rayment, I. (1995) *Biophys. J. 68*, 19s−28s.
53. Berger, C. L., and Thomas, D. D. (1991) *Biochemistry 30*, 11036−11045.
54. Sleep, J. A., Hackney, D. D., and Boyer, P. D. (1980) *J. Biol. Chem. 255*, 4094−4099.
55. Webb, M. R., and Trentham, D. R. (1981) *J. Biol. Chem. 256*, 10910−10916.
56. Dale, M. P., and Hackney, D. D. (1987) *Biochemistry 26*, 8365−8372.
57. Schweins, T., Langen, R., and Warshel, A. (1994) *Nat. Struct. Biol. 1*, 476−484.
58. Schweins, T., Geyer, M., Scheffzek, K., Warshel, A., Kalbitzer, H. R., and Wittinghofer, A. (1995) *Struct. Biol. 2*, 36−44.
59. Schweins, T., Geyer, M., Kalbitzer, H. R., Wittinghofer, A., and Warshel, A. (1996) *Biochemistry 35*, 14225−14231.
60. Kabsch, W. (1976) *Acta Crystallogr. A 32*, 922−923.
61. Kraulis, P. J. (1991) *J. Appl. Crystallogr. 24*, 946−950.

BI9712596